NANO LETTERS

2009
Vol. 9, No. 11
3922-3929

Plasmonic Nanogalaxies: Multiscale Aperiodic Arrays for Surface-Enhanced Raman Sensing

Ashwin Gopinath,[†] Svetlana V. Boriskina,[†] W. Ranjith Premasiri,[‡] Lawrence Ziegler,[‡] Björn M. Reinhard,[‡] and Luca Dal Negro*[,†]

Department of Electrical and Computer Engineering & Photonics Center, Boston University, 8 Saint Mary's Street, Boston, Massachusetts 02215-2421, and Department of Chemistry, Boston University, 590 Commonwealth Avenue, Boston, Massachusetts 02215

Received July 4, 2009; Revised Manuscript Received August 30, 2009

ABSTRACT

The accurate and reproducible control of intense electromagnetic fields localized on the nanoscale is essential for the engineering of optical sensors based on the surface-enhanced Raman scattering (SERS) effect. In this paper, using rigorous generalized Mie theory (GMT) calculations and a combined top-down/bottom-up nanofabrication approach, we design and experimentally demonstrate $\sim 10^8$ spatially averaged, reproducible SERS enhancement in deterministic aperiodic arrays of Au nanoparticles with different length scales. Deterministic aperiodic arrays of 200 nm diameter nanocylinders are first fabricated using electron-beam lithography on quartz substrates, and smaller size (30 nm diameter) Au nanoparticles are subsequently positioned by in situ Au reduction at regions of maximum field enhancement. These multiscale structures, which we call "plasmonic nanogalaxies", feature a cascade enhancement effect due to the strong electromagnetic interactions of small satellite nanoparticles with localized fields in aperiodic arrays of nanocylinders. The development of SERS substrates based on aperiodic arrays with different length scales provides a novel strategy to engineer plasmon-enhanced biosensors with chemical fingerprinting capability.

Introduction. Surface-enhanced Raman scattering is one of the most promising applications of the enhanced optical fields generated by the excitation of localized surface plasmon modes in the proximity of metal nanostructures. The SERS spectrum reveals the vibrational modes of the target molecules, thus conveying specific information with fingerprinting accuracy. Furthermore, the sensitivity of SERS measurements is one of the highest among analytical techniques, potentially leading to single molecule detection.[1,2]

While the SERS signal from a particular molecule is affected by both chemical and electromagnetic contributions,[3] it is now widely accepted that the dominant factor in SERS sensing results from the electromagnetic local field enhancement due to the resonant excitation of localized plasmon modes in metal nanostructures.[4,5] Therefore, in the field of SERS spectroscopy it is essential to engineer high electromagnetic fields with reproducible characteristics on metal−dielectric nanostructures. Traditionally, SERS enhancement has often been achieved using chemically prepared metal nanoparticle aggregates and roughened metal surfaces, which are both examples of random systems described by statistical fractal models.[6,7] Using these nanoparticle aggregates, characterized by scale invariant interactions[6,7] and extremely small interparticle separations,[8] large values of SERS enhancement ($\sim 10^{12}-10^{14}$) resulting in single molecule detection sensitivity under conditions of electronic enhancement were reported. More recently, similar SERS substrates have also been used to demonstrate label-free detection of explosives,[9,10] protein binding and hybridization events,[11,12] and viral particle and bacterial cell detection.[13−17]

However, all these approaches rely on localized surface plasmons in nanoparticle aggregates with random morphologies, suffering from lack of reproducibility and the absence of simple engineering design rules. Therefore, there is currently a strong need for "rationally designed", strongly enhancing planar SERS substrates fabricated using reproducible nanolithographic approaches, enabling the engineering of localized fields on the nanoscale. In this effort, electron-beam lithography (EBL) is an ideal method for the fabrication of SERS substrates owing to the ability to accurately control the shape, size, and morphology of structures down to ∼15 nm. Experimentally measured ensemble-averaged Raman enhancements of 10^4-10^6 have been recently demonstrated from substrates produced by EBL.[18−20] Although feature sizes in the 1−5 nm range, which are attainable with chemically fabricated substrates, cannot be written using EBL lithography, the reproducibility of the EBL technique provides a high level of control of nanoparticle positions, morphologies,

* Corresponding author: dalnegro@bu.edu.
[†] Department of Electrical and Computer Engineering & Photonics Center, Boston University.
[‡] Department of Chemistry, Boston University.

10.1021/nl902134r CCC: $40.75
Published on Web 09/15/2009

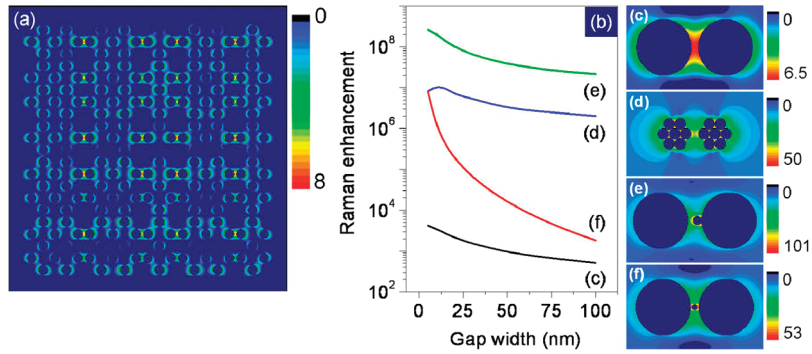

Figure 1. (a) Electric field distribution featuring hot spots in the array of 200 nm diameter Au nanospheres arranged according to the Fibonacci sequence with minimum interparticle separation of 50 nm illuminated by an *x*-polarized plane wave at $\lambda = 785$ nm. (b) Raman enhancement in a dimer and in various multiscale structures as a function of the interparticle gap width (w). The geometries and the field distributions in (c) a dimer ($w = 25$ nm), (d) a nanocluster dimer ($w = 25$ nm), (e) a 200 nm diameter dimer with a 50 nm separation and a 30 nm diameter nanosatellite attached to one of the spheres ($w = 19$ nm), and (f) a 200 nm diameter dimer with a 20 nm diameter satellite positioned between two spheres separated by 30 nm ($w = 5$ nm).

and array geometries. In particular, the accurate control of nanoparticle positions enables the design and engineering of "structural field enhancement effects" induced by the interplay of far-field electrodynamical interactions (diffractive modes) and near-field electrostatic coupling (lighting rod effect) in arrays of metal nanoparticles with complex geometries. Our recent computational and experimental work has demonstrated engineered structural field enhancement in deterministic aperiodic nanoparticle arrays with minimum interparticle separations of 25 nm, resulting in the formation of reproducible electromagnetic hot spots with up to $\sim 10^5$ and 10^7 spatially-averaged SERS enhancement factors in aperiodic arrays of nanocylinders and nanotriangles, respectively.[21,22]

Large values of SERS enhancement have also been reported for a number of substrates fabricated by bottom-up techniques, including plasmonic core−shell nanoparticles,[23] nanoflowers, nanoplanets, and nanolenses.[24−26] Common to all these approaches is the presence of sharp metal features and/or synergistic multiscale plasmonic interactions. The highest SERS enhancement factor $\sim 10^{13}$ has been in fact predicted for a three-particle system called "electromagnetic nanolens",[26−30] and attributed to a cascade enhancement effect. In this system, the local optical field of a large metal nanoparticle, enhanced by the excitation of a surface plasmon mode, acts as the local excitation field for the smaller nanoparticles, leading to a further boost of the field enhancement. The key idea behind this approach is to induce a successive transfer of electromagnetic energy at multiple length scales that leads to extremely large field concentration. Metal nanolenses have been recently fabricated by laser ablation[26] as well as by using DNA templates,[30] and the experimentally measured enhancement factors in these nanostructures are $\sim 10^9$. However, these fabricated nanostructures are formed in an aqueous solution which limits their practical applicability.

In this paper, we introduce novel SERS substrates termed "aperiodic nanogalaxies", in which aperiodic metal nanoparticle arrays fabricated by EBL are decorated with smaller nanoparticles at predefined locations to initiate a cascade enhancement effect (nanolensing). Differently from previous approaches based on nanolens fabrication,[26,30] our method enables the realization of multiscale nanostructures on planar reproducible substrates by using conventional nanofabrication techniques. Aperiodic nanogalaxies provide large and reproducible Raman enhancements by combining two electromagnetic field enhancement mechanisms: long-range diffractive coupling (multiple light scattering) and cascaded near-field enhancement effects in multiscale deterministic aperiodic structures. Our experimental Raman measurements reveal that highly reproducible *spatially averaged* Raman enhancement factors on the order of 10^8 can be achieved using aperiodic nanogalaxies. The experimental measurements are fully rationalized within a semianalytical electrodynamical treatment based on the generalized Mie theory.[31]

Cascade Field Enhancement in Multiscale Aperiodic Structures. We have previously demonstrated theoretically[22,32] and experimentally[21,22] that deterministic aperiodic metal nanoparticle arrays fabricated by EBL can be used for the generation of highly localized optical fields at predefined locations in a wide frequency range.[33] The experimentally measured SERS enhancement from *p*-mercaptoaniline (pMA) molecules in different (Fibonacci, Thue-Morse and Rudin-Shapiro) aperiodic arrays of Au nanoparticles are approximately a factor of ~ 10 larger than those observed in periodic arrays with comparable particle sizes and separations.[22] Electromagnetic simulations (see Figure 1a) confirmed by NSOM measurements[21,22] of the electric field distribution in aperiodic Fibonacci arrays have revealed deterministic patterns of well-defined hot spots localized in the gaps between dimer-like structures. These aperiodic hot-spot distributions are explained by the interplay of short-range plasmonic coupling with the excitation of long-range photonic−plasmonic resonant modes.[22,34]

Here we show that by positioning smaller size nanoparticles overlapping the hot-spot locations in aperiodic nanoparticle arrays we can significantly boost the local electric fields through cascade enhancement effects similar to nano-

lensing. In order to explore the feasibility of the proposed approach, we first performed rigorous GMT electrodynamical calculations of the local field distributions and Raman enhancement scaling, estimated as in ref 22, for different multiscale dimer structures at $\lambda = 785$ nm. This computational approach provides an analytical solution to the full-vector Maxwell's equations, including retardation effects and all the necessary multipolar orders, enabling the most accurate treatment of both the near and the far-field responses of nanoparticle arrays of nanospheres arranged in arbitrary geometries.

Figure 1a shows the calculated hot-spots distribution for a Fibonacci nanoparticle array with 200 nm diameter Au nanoparticles and 50 nm minimum interparticle separation. This structure exhibits a regular hot-spot lattice of dimer junctions with local fields enhanced by both quasi-static interactions and long-range multiple scattering, as discussed in refs 21 and 22. In order to reduce the computational complexity, here we discuss cascade enhancement effects in nanoparticle dimer structures. A more general analysis can be performed on multiparticle deterministic aperiodic structures, at increased computational cost, without affecting the main design conclusions presented in this section.

In Figure 1b we compare the gap scaling of the Raman enhancement in proximity to a nanoparticle dimer (Figure 1c) with the behavior of various multiscale dimer-like structures. The first multiscale structure we consider is a dimer of nanoparticle clusters (Figure 1d), which has been recently demonstrated experimentally using periodic nanoparticle cluster arrays (NCAs).[35] The other two multiscale structures considered are nanosphere dimers decorated with a smaller satellite particle either attached to one of the spheres (Figure 1e) or positioned at midgap (Figure 1f). In order to study a configuration with attached nanosatellites, which corresponds to the local geometry of the experimental substrates employed in this study, we positioned the satellite nanoparticle in the dimer junction 1 nm away from the surface of one of the large particles. This choice of interparticle separation results from the fact that classical electromagnetic GMT simulations cannot be reliably used for shorter interparticle distances, due to the increasing importance of nonlocal quantum effects at such short separations.[36] In Figure 1b we study the scaling of the local field enhancement for different multiscale structures as a function of the dimer gap width. The gap width is measured as the edge-to-edge separation between two nanospheres (Figure 1c), between two nanoparticle clusters (Figure 1d), or between the smaller and a larger nanoparticles for the dimers decorated with nanosatellites (Figure 1e,f). The results presented in Figure 1b for all the structures clearly demonstrate the merit of the multiscale approach, which results in the field enhancement values exceeding by 3 to 4 orders of magnitude the enhancement achieved in a bare nanoparticle dimer. We also found that the Raman enhancement increases nonlinearly with narrowing interparticle gaps, and the largest enhancement is predicted for the dimer structures decorated with a smaller nanoparticle satellite, since the presence of different length scales strongly focuses the plasmonic local

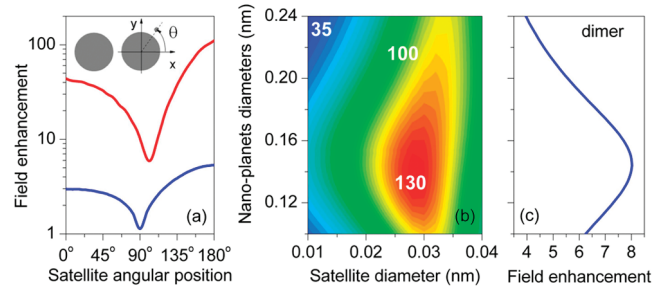

Figure 2. (a) Maximum electric field enhancement in a dimer of 200 nm diameter Au nanoparticles (nanoplanets) separated by a 50 nm gap and decorated with a 30 nm diameter Au nanosatellite attached to one of the larger spheres as a function of the satellite angular position (red). For comparison, the field enhancement on a periphery of an undecorated dimer measured 1 nm away from the sphere surface is also shown as a function of the angular position (blue). The inset shows the schematic of the decorated dimer and the used coordinate system. (b) Field enhancement in a dimer decorated with a satellite located at $\theta = 180°$ as a function of the nanoplanets and the satellite diameter. The absolute values of the electric field are shown as white labels on the contour plot. (c) Field enhancement in the undecorated dimer as a function of the nanoplanets diameters. All the structures are illuminated by an x-polarized plane wave at $\lambda = 785$ nm.

fields around the smaller particle. As shown in Figure 1e, the strongest field enhancement is always observed when particles are nearly touching (Figures 1d−f). Consequently, the steepest enhancement scaling with gap widths can be observed for the dimer decorated with a satellite at the center, while smoother scaling laws are observed in all other cases, which are already closer to the optimal geometry.

The results shown in Figure 1d also demonstrate that the Raman enhancement in NCAs (nanocluster dimer)[35] is dominated by the short-distance quasi-static electromagnetic coupling between the particles inside each cluster. We anticipate that the symmetry of the NCAs can also play a crucial role in determining the overall field enhancement. Here for simplicity we considered hexagonal close packed NCAs as recently demonstrated experimentally.[34] Interestingly, our data show that the enhancement in the NCAs reaches a maximum at ~10 nm intercluster separation and subsequently decreases for smaller ones. This behavior is attributed to the formation of delocalized plasmonic modes, which couple the entire NCA volumes at separations smaller than 10 nm.

The performances of the considered multiscale structures can be further optimized by tuning the relative positions and sizes of the nanoparticles. In Figure 2 we show this optimization in the case of satellite-decorated dimer structures which show the largest enhancement for all the gap separations (Figure 1b). In Figure 2a we compare the field enhancement of an incident plane wave ($\lambda = 785$ nm) in the vicinity of a dimer (200 nm diameter spheres) with the one observed by positioning a 30 nm nanosatellite in the dimer local field at different angular positions. The plots in Figure 2a correspond to the field enhancement probed 1 nm away from the surface of one of the larger spheres (blue) and the maximum value of field enhancement on the dimer

decorated with a smaller particle (red). It can be seen in Figure 2a that the angular trend of the enhancement remains approximately the same in both cases (the slight shift of the red curve is due to the fact that the maximum enhancement occurs on the surface of the satellite rather than at its center). Analogously, parts b and c of Figure 2 show the same trend of the enhancement scaling with the sizes of larger spheres in the bare and the decorated dimers. We conclude that, differently from the case of NCAs, where short-range quasi-static coupling dominates the field enhancement, the electromagnetic response of the decorated dimer structures is driven by the focusing of plasmonic local fields around the smaller particle, resulting in a cascade enhancement more similar to the nanolensing case. The presence of the nanosatellite does not significantly affect the overall spatial field pattern in the dimer, as the polarizability of the satellite (proportional to its volume) is significantly smaller than that of the larger nanoparticles. Therefore, on the basis of our analysis we anticipate that the multiscale approach can further enhance the field intensity in the hot spots of aperiodic arrays of metal nanoparticles, which are additionally strongly influenced by long-range diffractive coupling,[21,22,32,33] while keeping the deterministic character of the hot spots distributions virtually unchanged. In the next sections, we will experimentally demonstrate the feasibility of the proposed design and quantitatively assess its SERS performances.

Fabrication. The aperiodic nanogalaxy structures were fabricated by employing a combination of top-down e-beam nanolithography to define Fibonacci, Thue-More, and Rudin-Shapiro arrays of nanocylinders (200 nm diameter, 30 nm height) with separations ranging between 25 and 100 nm followed by bottom-up in situ chemical Au reduction to attach smaller nanoparticles (satellites). These three aperiodic structures are the representative examples of the three main classes of deterministic aperiodic systems, and their plasmonic scattering properties have been investigated in detail elsewhere.[22,32,34,37,38] A reference periodic structure consisting of a square-lattice periodic array has also been fabricated for comparison. A 180 nm thick layer of PMMA (poly(methyl methacrylate)) was spin-coated on top of the cleaned substrate (quartz microscope slide with 10 nm of ITO for conduction). The aperiodic nanopatterns were defined using a Zeiss SUPRA 40 VP scanning electron microscope equipped with a Raith Beam Blanker and nanometer pattern generation system (NPGS) with current and area dosage of 38 pA and 400 μC/cm^2, respectively. After the resist was developed in a 1:3 solution of MIBK (methyl isobutyle ketone) and IPA (isopropanol), a 30 nm thick Au film was deposited on the patterned surface by electron-beam evaporation. Finally, liftoff was performed using acetone leaving the designed Au nanoparticle arrays. The representative scanning electron micrograph of the Fibonacci nanoparticle array, which exhibits the highest SERS enhancement,[22] is shown in Figure 3a. The particle diameter is 200 nm, and the minimum interparticle separation is 25 nm. Subsequently, the fabricated chips consisting of periodic and aperiodic arrays were cleaned by RCA1 solution ($NH_4OH + H_2O_2 + H_2O$) in order to remove any organic residue from the e-beam

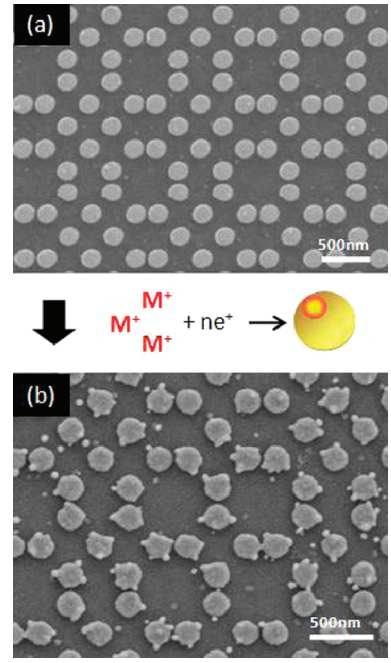

Figure 3. (a) Fibonacci nanocylinder array fabricated by e-beam lithography with particle diameter of 200 nm and minimum interparticle separation of 25 nm. (b) Fibonacci nanogalaxy formed by the adhesion of smaller satellite nanoparticle of 30 nm diameter .

fabrication procedure. The smaller gold nanoparticles were produced by an in situ growth procedure.[14,17] An aqueous solution of gold salt was formed by dissolution of 50 μL of $HAuCl_4$ (1 M $HAuCl_4$ 99.99% Sigma) in 100 mL of Millipore water. Subsequently, 25 mL of 2.5 mM aqueous solution of $NaBH_4$ was added dropwise to the gold chloride solution while being stirred constantly at 50 rpm The cleaned chips with the aperiodic Au nanoparticle arrays were submerged in the nanoparticle growth solution and were placed in a refrigerator for 24 h. The resulting nanostructured SERS substrates consist of large-scale, e-beam defined metal nanoparticle arrays decorated by smaller nanoparticles selectively grown on the particles and interstitial gap locations, as shown in Figures 3b and 5.

This fabrication process results in nanostructures whose features can be well controlled. The dimensions and positions of the large nanoparticles are controlled precisely by e-beam lithography. The nanosatellites on the gold particles can potentially be tuned by modification of the in situ nanoparticle growth procedure.[14,17]

The inherent randomness of the attachment locations of the smaller nanoparticles over the e-beam defined larger ones is not a serious cause of concern as this inhomogeneity is restricted to a very small region around the position of the larger particles. Moreover, we notice that in arrays with typically more than 2000 large nanoparticles, the probability of a favorable arrangement within the nanoparticle arrays for optimum SERS enhancement is expected to be very large. A similar strategy consisting of the attachment of multiple small satellites particles to a larger one was recently demonstrated and referred to as a "plasmonic nanoplanet".[25]

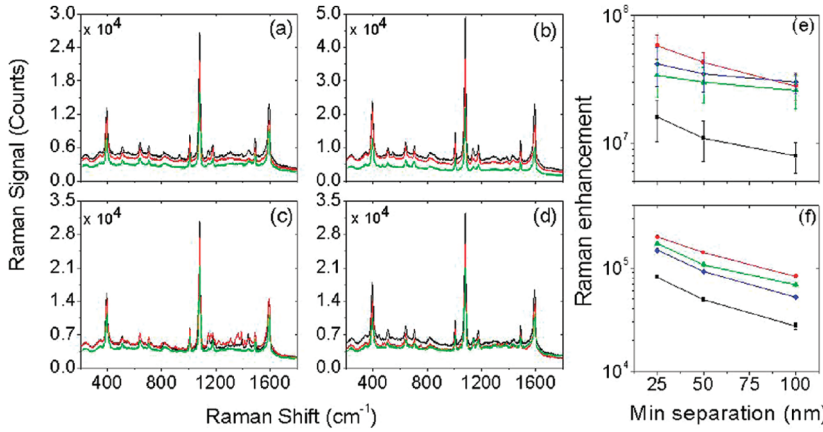

Figure 4. Experimental stokes SERS spectra of pMA on periodic (a), Fibonacci (b), Thue−Morse (c), and Rudin−Shapiro (d) nanogalaxies with lithographically defined minimum interparticle separation 25 nm (black), 50 nm (red), and 100 nm (green). The scaling behavior of Raman enhancement factor calculated from experimental data in periodic (black), Fibonacci (red), Thue−Morse (green), and Rudin−Shapiro (blue) nanogalaxies (e) and corresponding undecorated nanoparticle arrays (f). Each point in the figure is an average over six different substrates for a given geometry and interparticle separation. The introduction of the satellite nanoparticle leads to almost 3 orders of magnitude increase in the enhancement factor without significant perturbation of the scaling behavior.

One of the main goals of this work was to facilitate the adhesion of the small nanoparticles onto the larger ones without using any chemical functionalization step in order to avoid residual chemical impurities, which could interfere with the SERS signal. In our fabrication method, the smaller nanoparticles are directly attached to the larger particles forming a chemical-free nanostructure.[39−41]

pMA Measurements on Aperiodic Nanogalaxies. The SERS measurements on the fabricated periodic and aperiodic nanogalaxies were performed using pMA (*p*-mercaptoaniline) due to its ability to form a molecular monolayer over Au surfaces,[23] enabling the unambiguous quantification of the SERS enhancement factor per molecule. The Raman measurements were performed using a Renishaw InVia Raman instrument operating at 785 nm in a back reflection mode and equipped with a 50× objective (N.A. = 0.75). SERS data were acquired using an integration time of 10 s and incident laser power of 0.67mW. Parts a−d of Figure 4 show the Stokes Raman spectra of homogeneous pMA monolayers formed on the Au periodic and aperiodic nanogalaxies with different interparticle separations. The three dominant Stokes modes (390, 1077, 1590 cm^{-1}), due to the bending and stretching modes of benzene rings in the pMA molecules,[23] are clearly observed in all the spectra. The quantitative comparison of the SERS efficiencies of different arrays is performed by the analysis of the relative intensities of the 1077 cm^{-1} pMA Raman modes as discussed elsewhere.[23] The experimentally measured, spatially averaged SERS enhancement factors for different arrays are calculated with respect to the reference Raman signal per molecule measured on a homogeneous pMA bulk crystal using the following relation[23]

$$G_{SERS} = \frac{RS_{EN}N_{REF}}{RS_{REF}N_{EN}} \quad (1)$$

Here, RS_{EN} is the measured SERS signals from the plasmonic nanogalaxies and N_{EN} is the number of molecules on the arrays contributing to the measured signal. RS_{REF} and N_{REF} are the analogous quantities measured from the reference pMA sample in the absence of the SERS substrate. These quantities are calculated using the formula[23]

$$N_{REF} = \frac{B_v D_{pMA} A}{M_{pMA}} \quad (2)$$

where B_v is the optical excitation volume (2.5 μm × 25 μm × 5 μm), D_{pMA} is the density of pMA (1.06 g/cm^3) in the reference bulk crystal, A is the Avogadro number, and M_{pMA} is the molecular weight of pMA (125.19 amu). Due the ability of pMA molecules to form a monolayer on Au surface, the number of molecules contributing to the SERS effect (N_{EN}) can be estimated by the ratio of the total Au surface illuminated by the laser beam and the geometrical cross section of the individual pMA molecules (0.3 nm^2 per molecule).[42] While the estimation of the total illuminated Au surface is straightforward and accurate for SERS substrates entirely fabricated by e-beam lithography, in the case of plasmonic nanogalaxies this estimation requires certain assumptions. From the scanning electron microscopy (SEM) pictures of the fabricated nanogalaxies shown in Figure 1b, the average number of smaller nanoparticles which are attached to larger nanocylinders can be estimated to be 5. This information enables the calculation of the total covered Au surface area, which in turn gives the number of molecules contributing to the SERS signal. The enhancement factors calculated by this method are spatially averaged values and underestimate the local Raman enhancement experienced by the molecules located at the interparticle junctions. Although this procedure can lead to a drastic underestimation,[43,44] it represents a robust and reproducible method for the estimation of the SERS enhancement factors of complex multiscale arrays such as plasmonic nanogalaxies.

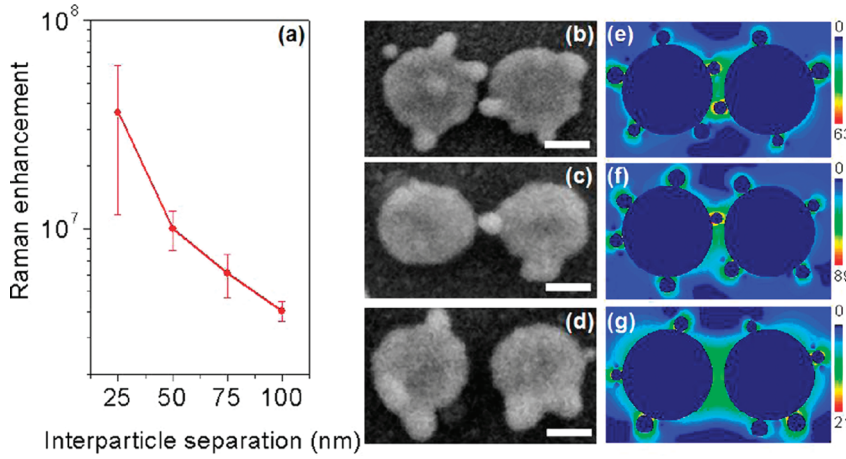

Figure 5. (a) Theoretically predicted maximum values of Raman enhancement in a dimer composed of 200 nm diameter Au nanospheres and decorated with smaller Au nanosatellites (a "double-star system"). (b−d) Characteristic SEM images of dimer-like structures in aperiodic nanogalaxy arrays, where the maximum field enhancement is expected. Three to six satellites of diameters ranging from 20 to 40 nm can be attached to larger particles at arbitrary positions. The scale bars on the SEM images are 100 nm in length. (e−g) The simulated electric field distributions in the nanostructures resembling (b−d) under the excitation by a horizontally polarized plane wave at $\lambda = 785$ nm.

In Figure 4e we show the SERS enhancement factors for the various nanogalaxies plotted with respect to the minimum interparticle separations of the e-beam defined nanocylinder arrays. Additionally, for comparison we show in Figure 4f the measured enhancement factors of identical aperiodic arrays in the absence of the small satellite nanoparticles. These data demonstrate directly that the selective attachment of smaller satellite nanoparticles leads to a dramatic increase of the SERS enhancement factors by 3 orders of magnitude without significantly perturbing the scaling behavior associated with the underlying deterministic aperiodic geometry, dictated by long-range diffractive coupling.[21,22,33,34,37] The reliability of this approach is demonstrated by noticing that each experimental point shown in Figure 4 is an average over six different substrates for a given geometry and interparticle separation. Additionally the cascaded field enhancement effects demonstrated experimentally in aperiodic plasmonic nanogalaxies (Figure 4) can be controlled and engineered by varying the geometry of the larger-scale aperiodic arrays. Finally, the large SERS enhancement factors $\sim 10^8$ experimentally measured in the case of the Fibonacci nanogalaxy only represent an underestimation of the local enhancement value since our calculation approach assumes that all the pMA molecules are equally contributing to the measured SERS signal. This assumption does not hold across the nanogalaxy substrates, and we can anticipate that the local enhancement can be significantly larger than 10^8 since only the satellite nanoparticles best located in the regions of maximum field enhancement dominate the overall SERS signal.

Near-Field Enhancement in the Presence of Randomness. Here we discuss the effects of structural randomness on the hot spots formation in aperiodic nanogalaxies based on GMT calculations. These simulations provide the *local* SERS enhancement values considering spherical nanoparticles, and thus they cannot be directly compared to *spatially averaged* SERS data experimentally measured for arrays of nanocylinders. However, as discussed in ref 22, the GMT analysis qualitatively supports the scaling behavior of the SERS enhancement data with respect to the interparticle separations.

We now investigate the *scaling* of calculated Raman enhancement values for decorated dimer structures with random satellite positions and sizes. In particular, we consider a nanoparticle dimer of 200 nm diameter particles and various gap distances between 25 nm and 100 nm (Figure 5a) with randomly attached smaller satellites of varying diameters (20−40 nm). This analysis enables the understanding of typical nanogalaxy morphologies where small Au nanosatellites attach at different locations around the larger EBL-defined posts. Parts b−d of Figure 5 show representative SEM pictures of dimer satellites in three nanogalaxy arrays with different interparticle separations. In order to account for this experimental situation, we considered in Figure 5a 10 different realizations of the randomly decorated dimer systems that form a double-star configuration of nanoparticles. Error bars are added in Figure 5a to quantitatively estimate the uncertainty in the calculated field values over different realizations. The field profiles corresponding to three different realizations of nanosatellites are shown in Figure 5, parts e−g. Interestingly, we notice by comparing the results in Figure 5a and Figure 1b for the bare nanoparticle dimer that similar SERS scaling with respect to the particle separation is observed, irrespective of the intrinsic randomness in the satellite attachment positions and sizes. In addition, Figure 5a demonstrates that even in the presence of randomness a dramatic (4 orders of magnitude) increase in the SERS enhancement can be achieved in nanogalaxies due to the multiscale field coupling. The predicted scaling behavior is preserved also in the more complex case of aperiodic arrays of decorated dimers (nanogalaxies) of nanocylinders, as demonstrated by the experimental data in Figure 4, parts e and f. We conclude that the proposed nanogalaxy approach enables robust and reproducible SERS sensing despite the presence of localized randomness in the satellite positions.

Conclusions. In this work, by combing top-down nanofabrication approach with a bottom-up fabrication technique, we successfully designed and fabricated a hybrid multiscale aperiodic nanostructure, called "aperiodic nanogalaxy", which resulted in $\sim 10^8 \pm 7.28\%$ spatially averaged, reproducible SERS enhancement. GMT-based electromagnetic simulations provided the physical rationale for our experimental results and clearly demonstrated the importance of cascaded field enhancement effects for the engineering of multiscale aperiodic structures and the development of high-sensitivity SERS substrates. Our combined computational and experimental study demonstrates that $\sim 10^8$ spatially averaged SERS enhancement values can be achieved in rationally designed planar plasmonic structures. Future work will focus on further substrate optimization by investigating nanoparticles with different shapes and smaller separations. The ability to accurately design and controllably fabricate plasmonic multiscale nanostructures with high and reproducible field-enhanced hot spots is quintessential for the development of the next generation SERS substrates.

Acknowledgment. The authors thank Drs. Y.-L. Xu and M. Ringler for making their Fortran codes available for public use. This work was partially supported by the US Army Research Laboratory under Contract Numbers W911NF-06-2-0040 and W911 NF-07-1-0618.

References

(1) Kneipp, K.; Wang, Y.; Kneipp, H.; Perelman, L. T.; Itzkan, I.; Dasari, R. R.; Feld, M. S. Single Molecule Detection Using Surface-Enhanced Raman Scattering (SERS). *Phys. Rev. Lett.* **1997**, *78* (9), 1667–1670.

(2) Nie, S.; Emory, S. R. Probing Single Molecules and Single Nanoparticles by Surface-Enhanced Raman Scattering. *Science* **1997**, *275* (5303), 1102–1106.

(3) Novotny, L.; Hecht, B. *Principles of Nano-Optics*; Cambridge University Press: Cambridge, 2006.

(4) Fleischmann, M.; Hendra, P. J.; McQuillan, A. J. Raman spectra of pyridine adsorbed at a silver electrode. *Chem. Phys. Lett.* **1974**, *26* (2), 163–166.

(5) Jeanmaire, D. L.; Van Duyne, R. P. Surface Raman spectroelectrochemistry: Part I. Heterocyclic, aromatic, and aliphatic amines adsorbed on the anodized silver electrode. *J. Electroanal. Chem.* **1977**, *84* (1), 1–20.

(6) Shalaev, V. M. Electromagnetic properties of small-particle composites. *Phys. Rep.* **1996**, *272* (2−3), 61–137.

(7) Stockman, M. I.; Shalaev, V. M.; Moskovits, M.; Botet, R.; George, T. F. Enhanced Raman scattering by fractal clusters: Scale-invariant theory. *Phys. Rev. B* **1992**, *46* (5), 2821.

(8) Hao, E.; Schatz, G. C. Electromagnetic fields around silver nanoparticles and dimers. *J. Chem. Phys.* **2004**, *120*, 357–366.

(9) Kneipp, K.; Wang, Y.; Dasari, R. R.; Feld, M. S.; Gilbert, B. D.; Janni, J.; Steinfeld, J. I. Near-infrared surface-enhanced Raman scattering of trinitrotoluene on colloidal gold and silver. *Spectrochim. Acta, Part A* **1995**, *51* (12), 2171–2175.

(10) Primera-Pedrozo, O. M.; Jerez-Rozo, J. I.; De La Cruz-Montoya, E.; Luna-Pineda, T.; Pacheco-Londoño, L. C.; Hernández-Rivera, S. P. Nanotechnology-Based Detection of Explosives and Biological Agents Simulants. *IEEE Sens. J.* **2008**, *8* (6), 963.

(11) Cao, Y. C.; Jin, R.; Mirkin, C. A. Nanoparticles with Raman Spectroscopic Fingerprints for DNA and RNA Detection. *Science* **2002**, *297* (5586), 1536–1540.

(12) Delfino, I.; Bizzarri, A. R.; Cannistraro, S. Single-molecule detection of yeast cytochrome c by Surface-Enhanced Raman Spectroscopy. *Biophys. Chem.* **2005**, *113* (1), 41–51.

(13) Shanmukh, S.; Jones, L.; Driskell, J.; Zhao, Y.; Dluhy, R.; Tripp, R. A. Rapid and Sensitive Detection of Respiratory Virus Molecular Signatures Using a Silver Nanorod Array SERS Substrate. *Nano Lett.* **2006**, *6* (11), 2630–2636.

(14) Premasiri, W. R.; Moir, D. T.; Klempner, M. S.; Krieger, N.; Jones, G.; Ziegler, L. D. Characterization of the Surface Enhanced Raman Scattering (SERS) of Bacteria. *J. Phys. Chem. B* **2005**, *109* (1), 312–320.

(15) Jarvis, R. M.; Goodacre, R. Discrimination of bacteria using surface-enhanced Raman spectroscopy. *Anal. Chem.* **2004**, *76* (1), 40–47.

(16) Jarvis, R. M.; Brooker, A.; Goodacre, R. Surface-enhanced Raman scattering for the rapid discrimination of bacteria. *Faraday Discuss.* **2006**, *132*, 281–292.

(17) Patel, I. S.; Premasiri, W. R.; Moir, D. T.; Ziegler, L. D. Barcoding bacterial cells: a SERS-based methodology for pathogen identification. *J. Raman Spectrosc.* **2008**, *39* (11), 1660–1672.

(18) Gunnarsson, L.; Bjerneld, E. J.; Xu, H.; Petronis, S.; Kasemo, B.; Kall, M. Interparticle coupling effects in nanofabricated substrates for surface-enhanced Raman scattering. *Appl. Phys. Lett.* **2001**, *78* (6), 802–804.

(19) Liu, Y. J.; Zhang, Z. Y.; Zhao, Q.; Zhao, Y. P. Revisiting the separation dependent surface enhanced Raman scattering. *Appl. Phys. Lett.* **2008**, *93* (17), 173106-3.

(20) Yu, Q.; Guan, P.; Qin, D.; Golden, G.; Wallace, P. M. Inverted Size-Dependence of Surface-Enhanced Raman Scattering on Gold Nanohole and Nanodisk Arrays. *Nano Lett.* **2008**, *8* (7), 1923–1928.

(21) Dallapiccola, R.; Gopinath, A.; Stellacci, F.; Dal Negro, L. Quasi-periodic distribution of plasmon modes in two-dimensional Fibonacci arrays of metal nanoparticles. *Opt. Express* **2008**, *16* (8), 5544–5555.

(22) Gopinath, A.; Boriskina, S. V.; Reinhard, B. M.; Dal Negro, L. Deterministic aperiodic arrays of metal nanoparticles for surface-enhanced Raman scattering (SERS). *Opt. Express* **2009**, *17* (5), 3741–3753.

(23) Jackson, J. B.; Halas, N. J. Surface-enhanced Raman scattering on tunable plasmonic nanoparticle substrates. *Proc. Natl. Acad. Sci. U.S.A.* **2004**, *101* (52), 17930–17935.

(24) Wang, T.; Hu, X.; Dong, S. Surfactantless synthesis of multiple shapes of gold nanostructures and their shape-dependent SERS spectroscopy. *J. Phys. Chem. B* **2006**, *110* (34), 16930–16936.

(25) Pellegrini, G.; Bello, V.; Mattei, G.; Mazzoldi, P. Local-field enhancement and plasmon tuning in bimetallic nanoplanets. *Opt. Express* **2007**, *15* (16), 10097–10102.

(26) Kneipp, J.; Li, X.; Sherwood, M.; Panne, U.; Kneipp, H.; Stockman, M. I.; Kneipp, K. Gold Nanolenses Generated by Laser Ablation-Efficient Enhancing Structure for Surface Enhanced Raman Scattering Analytics and Sensing. *Anal. Chem.* **2008**, *80* (11), 4247–4251.

(27) Li, K.; Stockman, M. I.; Bergman, D. J. Self-Similar Chain of Metal Nanospheres as an Efficient Nanolens. *Phys. Rev. Lett.* **2003**, *91* (22), 227402.

(28) Li, K.; Li, X.; Stockman, M. I.; Bergman, D. J. Surface plasmon amplification by stimulated emission in nanolenses. *Phys. Rev. B* **2005**, *71* (11), 115409.

(29) Li, K.; Stockman, M. I.; Bergman, D. J. Enhanced second harmonic generation in a self-similar chain of metal nanospheres. *Phys. Rev. B* **2005**, *72* (15), 153401.

(30) Bidault, S.; de Abajo, F. J. G.; Polman, A. Plasmon-Based Nanolenses Assembled O a Well-Defined DNA Template. *J. Am. Chem. Soc.* **2008**, *130*, 2750.

(31) Xu, Y.-l. Electromagnetic scattering by an aggregate of spheres. *Appl. Opt.* **1995**, *34* (21), 4573–4588.

(32) Forestiere, C.; Miano, G.; Rubinacci, G.; Dal Negro, L. Role of aperiodic order in the spectral, localization, and scaling properties of plasmon modes for the design of nanoparticle arrays. *Phys. Rev. B* **2009**, *79* (8).

(33) Forestiere, C.; Miano, G.; Boriskina, S. V.; Dal Negro, L. The role of nanoparticle shapes and deterministic aperiodicity for the design of nanoplasmonic arrays. *Opt. Express* **2009**, *17* (12), 9648–9661.

(34) Gopinath, A.; Boriskina, S. V.; Feng, N.-N.; Reinhard, B. M.; Dal Negro, L. Photonic-Plasmonic Scattering Resonances in Deterministic Aperiodic Structures. *Nano Lett.* **2008**, *8* (8), 2423–2431.

(35) Yan, B.; Thubagere, A.; Premasiri, W. R.; Ziegler, L. D.; Dal Negro, L.; Reinhard, B. r. M. Engineered SERS Substrates with Multiscale Signal Enhancement: Nanoparticle Cluster Arrays. *ACS Nano* **2009**, *3* (5), 1190–1202.

(36) Romero, I.; Aizpurua, J.; Bryant, G. W.; García De Abajo, F. J. Plasmons in nearly touching metallic nanoparticles: singular response in the limit of touching dimers. *Opt. Express* **2006**, *14* (21), 9988–9999.

(37) Dal Negro, L.; Ning-Ning, F.; Ashwin, G. "Electromagnetic coupling and plasmon localization in deterministic aperiodic arrays". *J. Opt. A: Pure Appl. Opt.* **2008**, (6), 064013.

(38) Dal Negro, L.; Feng, N.-N. Spectral gaps and mode localization in Fibonacci chains of metal nanoparticles. *Opt. Express* **2007**, *15* (22), 14396–14403.
(39) Mesquida, P.; Stemmer, A. Maskless nanofabrication using the electrostatic attachment of gold particles to electrically patterned surfaces. *Microelectron. Eng.* **2002**, *61−62*, 671–674.
(40) Flavel, B.; Nussio, M.; Quinton, J.; Shapter, J. , Adhesion of chemically and electrostatically bound gold nanoparticles to a self-assembled silane monolayer investigated by atomic force volume spectroscopy, *J. Nanopart. Res.*
(41) Liang, Z.; Susha, A.; Caruso, F. Gold Nanoparticle-Based Core Shell and Hollow Spheres and Ordered Assemblies Thereof. *Chem. Mater.* **2003**, *15* (16), 3176–3183.
(42) Mohri, N.; Matsushita, S.; Inoue, M.; Yoshikawa, K. Desorption of 4-Aminobenzenethiol Bound to a Gold Surface. *Langmuir* **1998**, *14* (9), 2343–2347.
(43) Wei, A.; Kim, B.; Sadtler, B.; Tripp, S. L. Tunable Surface-Enhanced Raman Scattering from Large Gold Nanoparticle Arrays. *ChemPhys-Chem* **2001**, *2*, 743.
(44) Garcia-Vidal, F. J.; Pendry, J. B. Collective Theory for Surface Enhanced Raman Scattering. *Phys. Rev. Lett.* **1996**, *77*, 1163.

NL902134R